Tsallis q-Gaussian function as fitting lineshape for Graphite Raman bands

Tsallis q-Gaussian function as fitting lineshape for Graphite Raman bands

Amelia Carolina Sparavigna

Department of Applied Science and Technology, Polytechnic University of Turin, Italy

Email: amelia.sparavigna@polito.it

Torino, July 16, 2023.

Abstract

Previous studies (Sparavigna, 2023) have demonstrated the Tsallis q-Gaussian functions suitable for the analysis of Raman spectra. These functions can be used for simulating the different lineshapes of Raman bands. Here we apply q-Gaussians to graphite Raman spectra from RRUFF and Raman Open Database.

Keywords: Tsallis q-Gaussian distribution, Gaussian distribution, Cauchy distribution, Lorentzian distribution, Raman spectroscopy, Graphite.

q-Gaussian functions, also known as Tsallis functions, are probability distributions proper of the Tsallis statistics (Tsallis, 1988, 1995, Hanel et al., 2009). The q-Gaussians are based on a generalized form of the exponential function (Sparavigna, 2022), characterized by a continuous parameter q in the range $1 < q < 3$.

As given by Umarov et al., 2008, the q-Gaussian function is $f(x) = Ce_q(-\beta x^2)$, where $e_q(.)$ is the q-exponential function and C a scale constant. In the exponent, we use $\beta = 1/(2\sigma^2)$, with variance σ. The q-exponential has expression: $exp_q(u) = [1 + (1-q)u]^{1/(1-q)}$. For q equal to 2, the q-Gaussian is the Cauchy-Lorentzian distribution (Naudts, 2009). For q close to 1, we have the usual Gaussian form. For the q-parameter between 1 and 2, the shape of the q-Gaussian function is intermediate between the Gaussian and the Lorentzian profile. This behavior turns the q-Gaussian into a function suitable for the analysis of Raman spectra, where the spectral bands are characterized, in the same manner, by intermediate profiles between Lorentzian and Gaussian outlines (Kirillov, 2004a). Besides these two functions, which remain the most popular for fitting Raman spectra, *linear combinations* (pseudo-Voigt distributions) or *convolutions* of them (Voigt distributions) are used too (Meier, 2005). The Voigtian function is essentially a Lorentzian height weighted by a Gaussian profile.

In spectroscopy, if the emission is broadened by the radiation damping, the profile of the band is Lorentzian. This profile can be modified by different mechanisms. Among them we have the thermal broadening that introduces a convolution with a Gaussian function, resulting in a consequent Voigt profile. "Alternatively, [we can] suppose that the line is scanned by a spectrophotometer with a Gaussian sensitivity function" (Tatum, 2022). In this case, the convolution of the line is with the instrumental function profile. Let us remember that "the general expression that takes account of all the instrumentally induced distortion of the true band shape can be called the *instrument function*" (Seshadri and Jones, 1963). It is also known as the "*instrumental transfer function*" (Merlen et al., 2017). Therefore, the true spectral distribution, subjected to "distortions both in the optical and recording parts of the apparatus" (Rautian, 1958), is replaced by the observed measured distribution. Besides the models based on the Voigtian convolution, different approaches exist (Kirillov, 2004b), so that the true radiation line can be assumed different from a Lorentzian function; moreover, the weight function can be different from a pure Gaussian function. In any case, it is always necessary to determine the instrumental function profile, at least to evaluate if its role is negligible; according to Merlen et al., 2017, the instrumental transfer function "can be negligible in many cases", and "depending on the grating used, the instrumental width varies but is in general close to 1 cm^{-1}."

With its intermediate behavior, the q-Gaussian is suitable to describe convolution mechanisms in general. In Sparavigna, 2023a, we have shown that the q-Gaussian is able of mimicking pseudo-Voigt and Voigt functions, and the same is true also for the Egelstaff-Schofield line shape (Sparavigna, 2023b). Besides a detailed discussion of the decomposition in bands of the Raman spectra for carbonaceous material, in Sparavigna, 2023c, we have shown several examples which demonstrate the q-Gaussians properly suitable for the Raman spectral data analysis. Here, we consider the q-exponential function for fitting onto the Raman spectrum of graphite. Data are considered from RRUFF collection (Lafuente et al., 2015) and from Raman Open Database, developed in the framework of project SOLSA H2020 (El Mendili et al., 2019). In the following plots, data are generally given in red and the best fits in green. The misfit is also proposed in the lower part of the images. Data and best fits are given as functions of integers *n* (equally spaced points), for the x-axis which is representing the Raman shift. A convenient scale is used for the y-axis (intensity axis).

RRUFF ID R050503 - Let us start considering graphite Raman spectrum RRUFF ID R050503. Graphite from Sterling mine, Ogdensburg, New Jersey, USA (Data source: Marcus Origlieri). The identification of this mineral has been confirmed by X-ray diffraction (RRUFF). The sample is unoriented, and the instrument settings are: Thermo Almega XR 532nm @ 100% of 150mW.

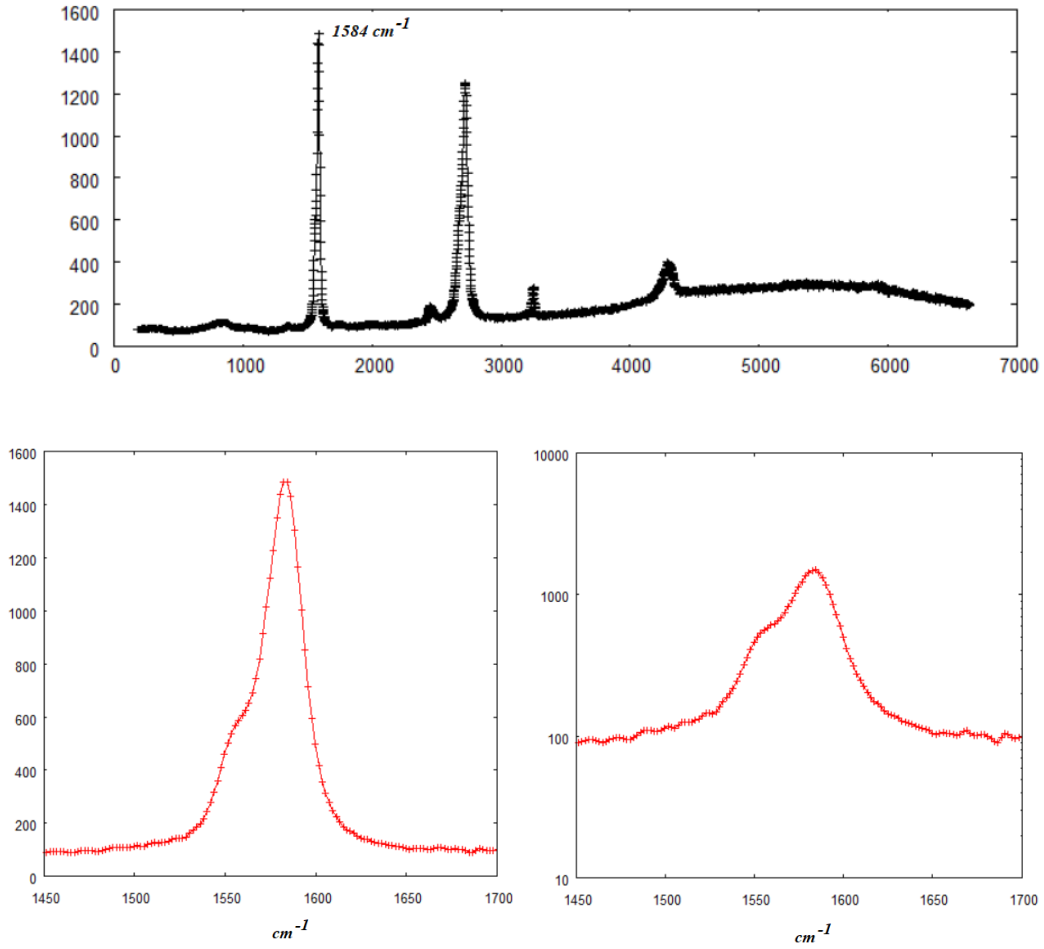

Fig. 1: Processed data of RRUFF ID R050503 (top). Peak at 1584 cm^{-1} (down). On the right, the data with log scale y-axis (semi log scale). In the considered frequency range, raw and processed data are the same.

We can note that data are ranging from intensity values of about 100 to the peak value of about 1500; it means that we have a base intensity of about 6% affecting the peak value. To fit this part of the graphite spectrum with a decomposition with two q-Gaussians, let us adjust the baseline, with a local linear baseline, according to intensities at 1450 and 1700 cm^{-1}.

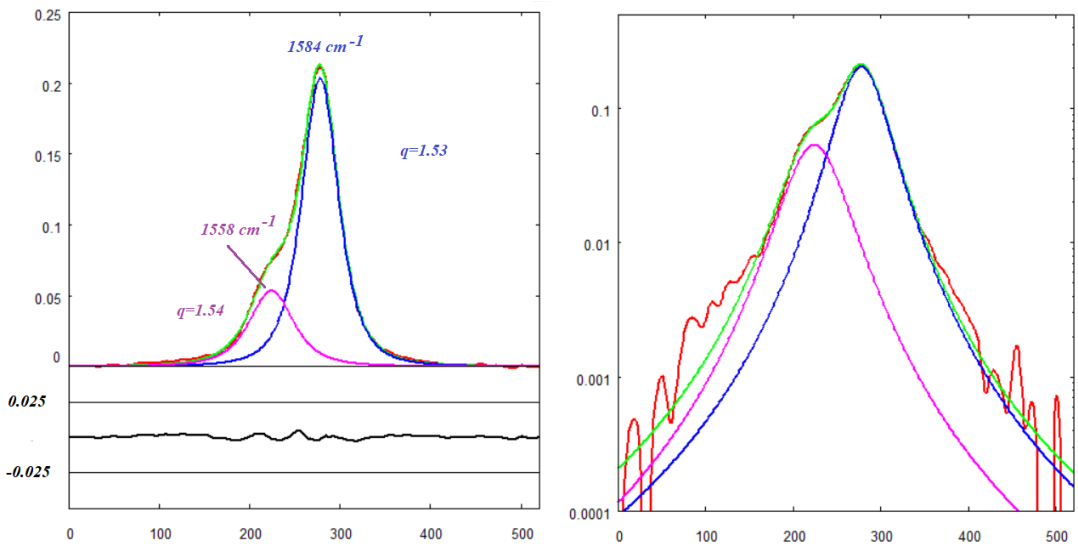

Fig. 2: The best fit (green) onto RRUFF ID R050503 Raman spectrum (red). Two q-Gaussians are used (the values of the q-parameters are given in the figure), The misfit is proposed in the lower part of the plot. On the right, the same fit is shown with the log scale for y-axis (semi log scale). Data and q-Gaussians are given as functions of integers n (equally spaced points), for the x-axis which is representing the Raman shift. A convenient scale is used for the y-axis (intensity axis). The fitting calculation is obtained by minimizing the sum of the squares of the deviations (sum from n=1 to n=520).

RRUFF ID R090047 - The second Raman spectrum that we consider is RRUFF ID R090047. Graphite from Merelani, Tanzania (Data source: Wendell Wilson). The identification of this mineral has been confirmed by X-ray diffraction (RRUFF). The sample is unoriented, and the instrument settings are: Thermo Almega XR 532nm @ 100% of 150mW.

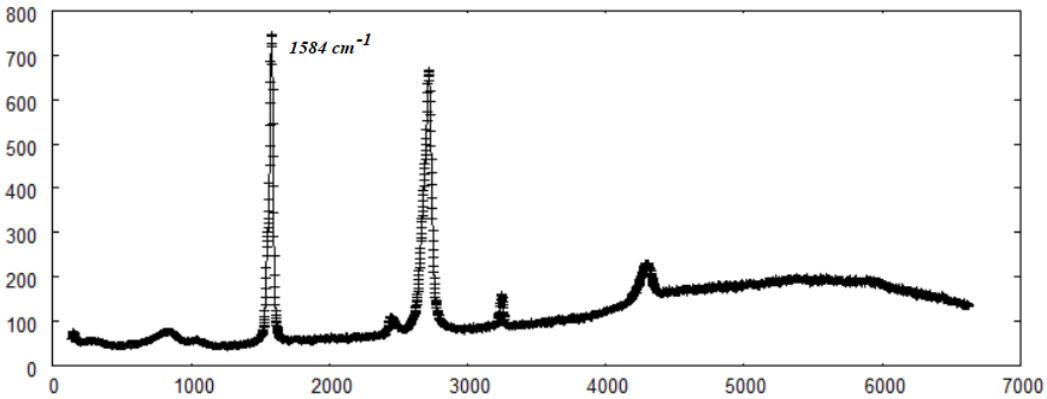

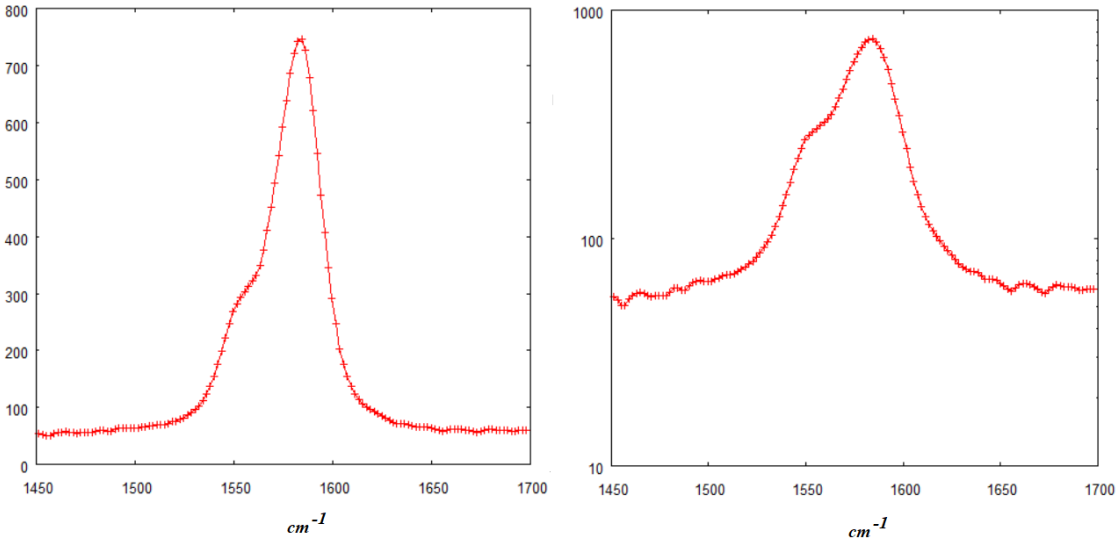

Fig. 3: Processed data of RRUFF ID R090047. Peak at 1584 cm^{-1} (down) On the right, the data with log scale y-axis.

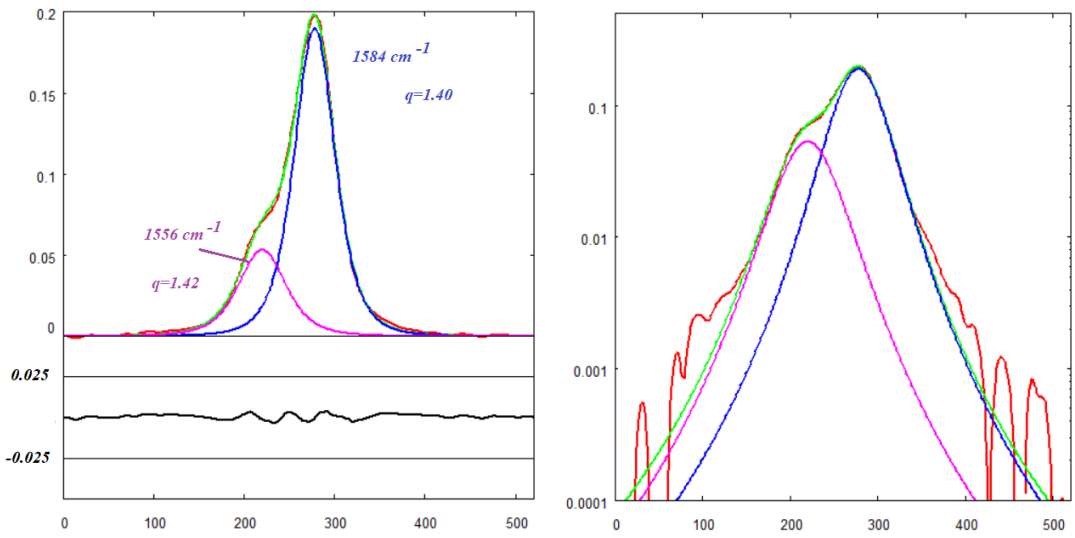

Fig. 4: The best fit (green) onto RRUFF ID R090047 and q-Gaussian components.

RRUFF ID R120025 - The third Raman spectrum that we find in RRUFF has ID number R120025. Graphite from Saint-Sauveur Graphite occurrence, Saint-Sauveur, Les Pays-d'en-Haut RCM, Laurentides, Québec, Canada (Data source: Donald Doell). The identification of this mineral is not yet confirmed (RRUFF). The sample is unoriented.

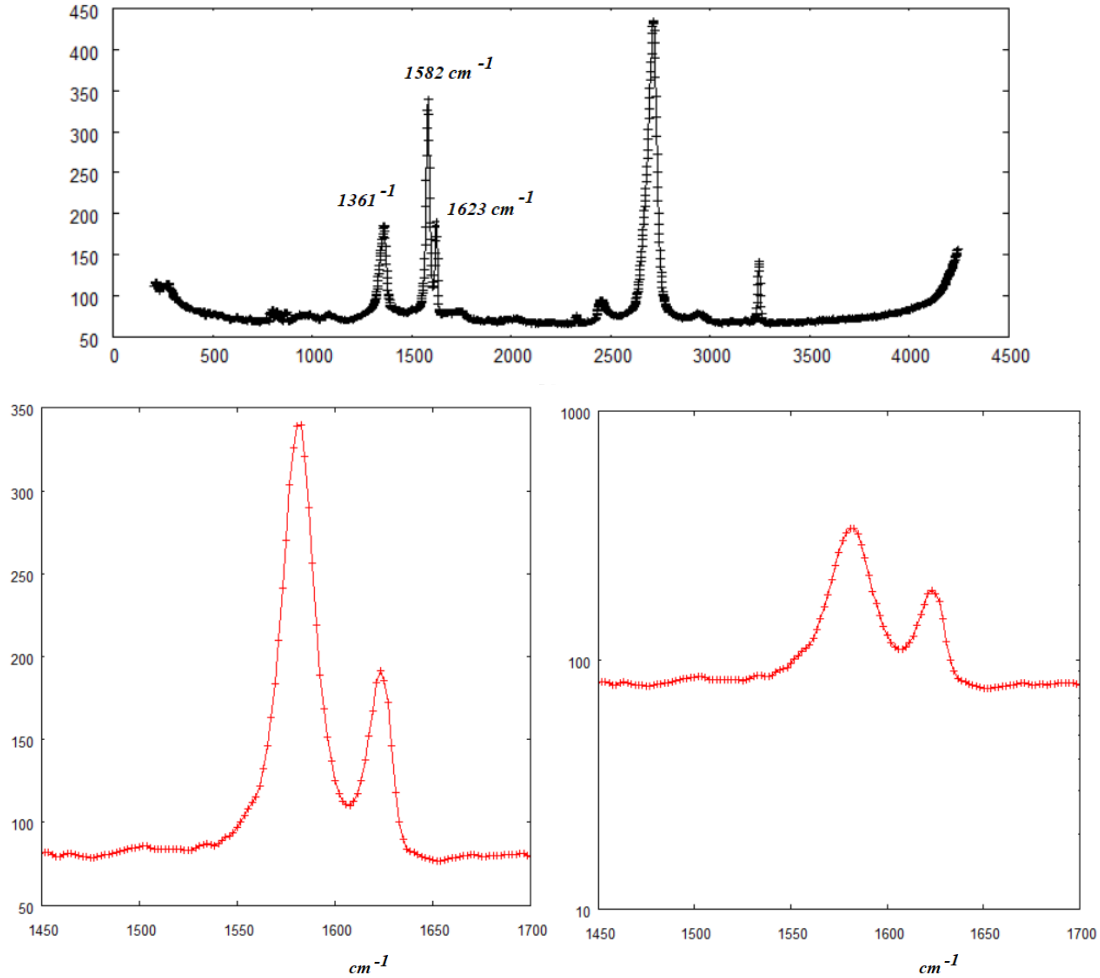

Fig. 5: Processed data of RRUFF ID R120025. On the right, the data with semi log scale.

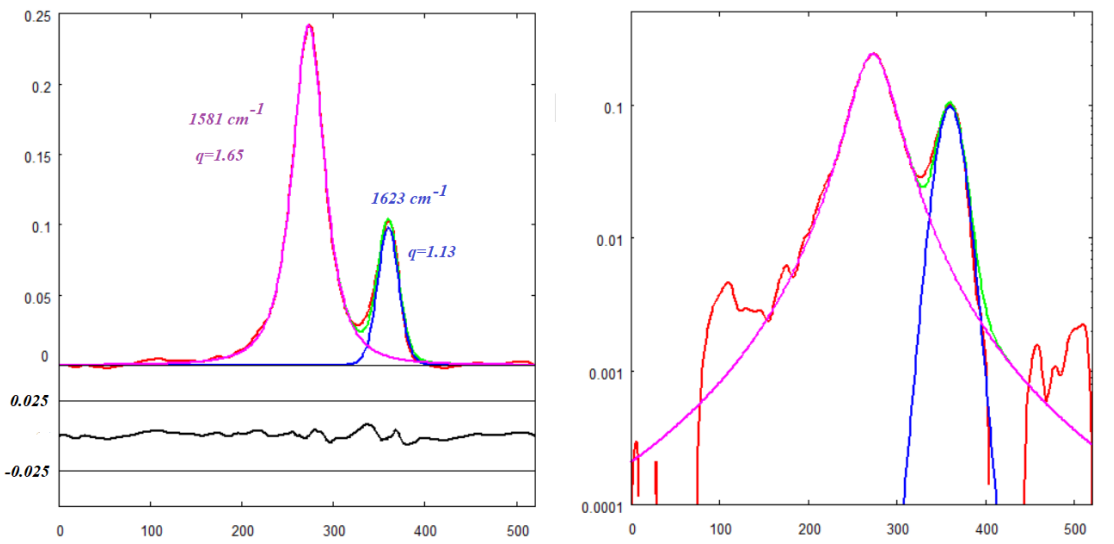

Fig. 6: The best fit (green) onto RRUFF ID R120025 and q-Gaussian components.

As we can see from Fig.6, the use of further components, such as at about 1500 and 1550 cm^{-1}, could further improve the fit, but this is beyond the aim of this discussion.

Raman Open Database entry n.3500021 - The Raman Open Database allows us to add a further Raman spectrum. The sample is graphite from Saint Laurent French reactors (author is Y. El Mendili, personal communication to ROD, 2018).

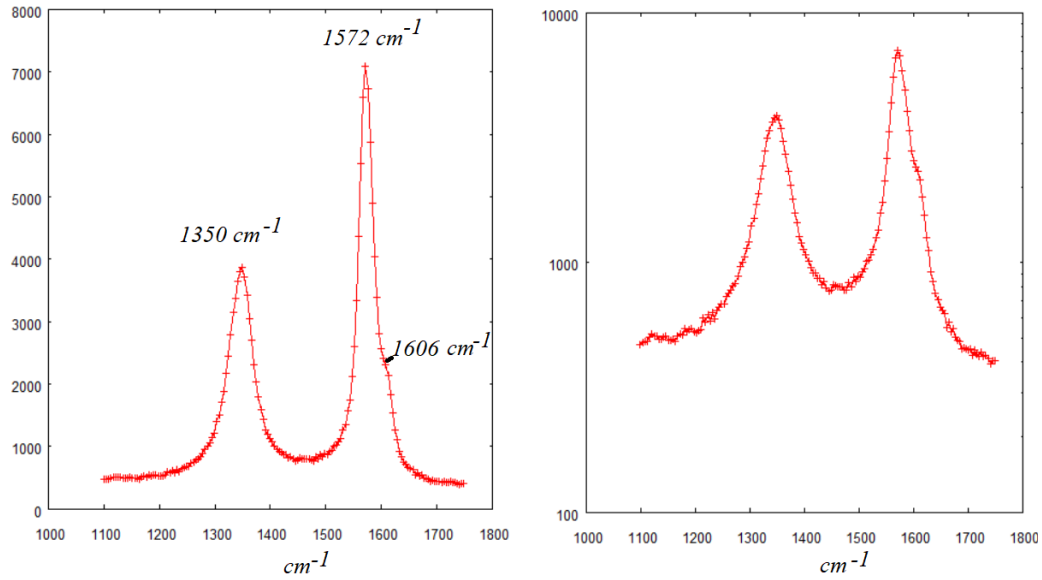

Fig. 7: Data of ROD 3500021. On the right, the data with log scale y-axis. On x-axis, we have Raman shift in cm^{-1}.

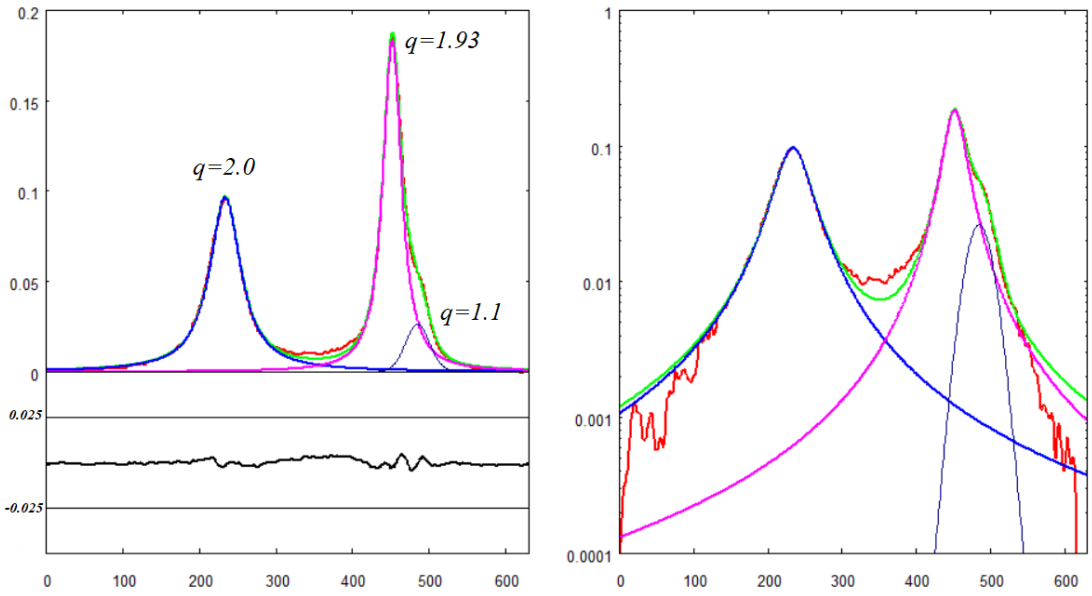

Fig. 8: The best fit (green) onto ROD 3500021 and three q-Gaussian components.

In the Fig.8, for the decomposition of the Raman spectrum we used three components. In the following Fig.9, the components are four. We added a component between the two main peaks.

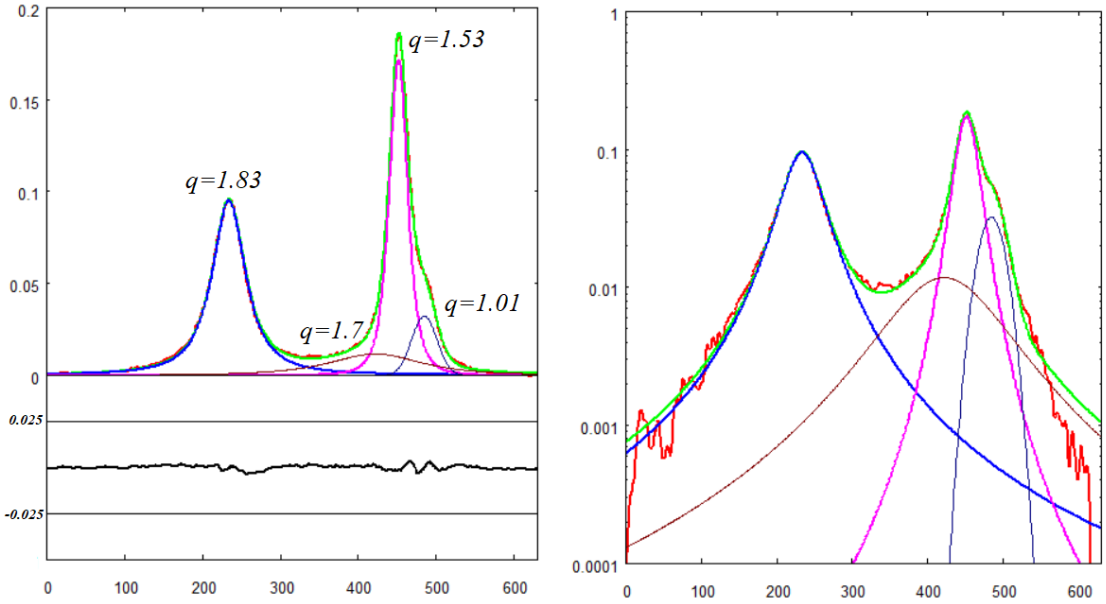

Fig. 9: The best fit (green) onto ROD 3500021 and four q-Gaussian components.

From the Fig.7, we can note that there is a shift of the main peak positions of about 10 cm^{-1}.

OSR2200 and OSR1500 – In Sparavigna, 2023a,c, we considered the q-Gaussians for the analysis of biochar, a carbonaceous material which is the solid residue of pyrolysis of biomass obtained by thermochemical decomposition at moderate temperatures under oxygen-limiting conditions (Brassard et al., 2019, Bartoli & Giorcelli, 2023). We used data collected by Tagliaferro et al., 2020. In the Figure 6 of their paper, we can find the Raman spectra for different samples. The carbonaceous material used by Tagliaferro and coworkers was a standardized biochar, subjected to pyrolysis at 550 °C, and then carbonized at various temperatures in the range 900–2200 °C. The Raman spectra were recorded with a 514 nm laser. Here we consider two Raman spectra from the Figure 6 of Tagliaferro et al., those of biochar carbonized at 2200 and 1500 °C. In the following figures, we show and decomposition with q-Gaussians are given.

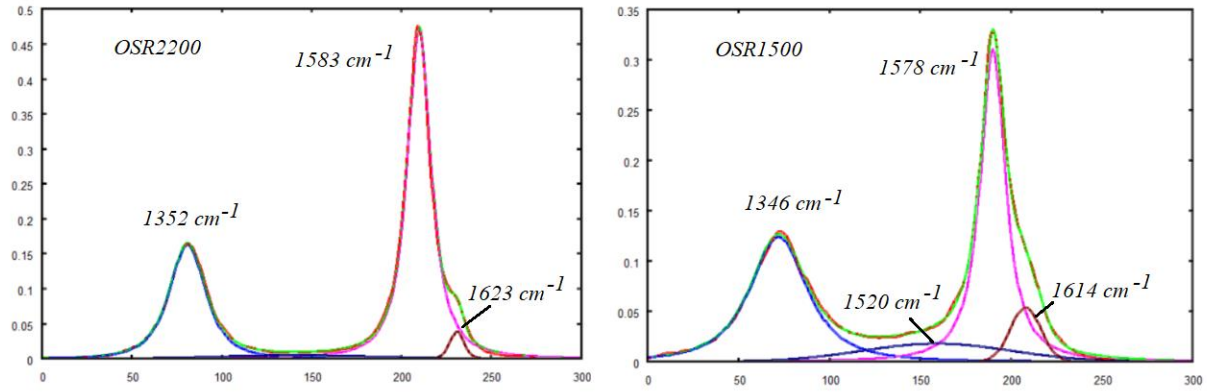

Fig.10 - On the left, data, and best fit q-Gaussian components of the Raman spectrum of OSR2200 (data from Tagliaferro et al., 2020, Fig.6f), on the right the same for the spectrum of OSR1500 (Fig.6d). The plots here proposed are the same as in Sparavigna, 2023c.

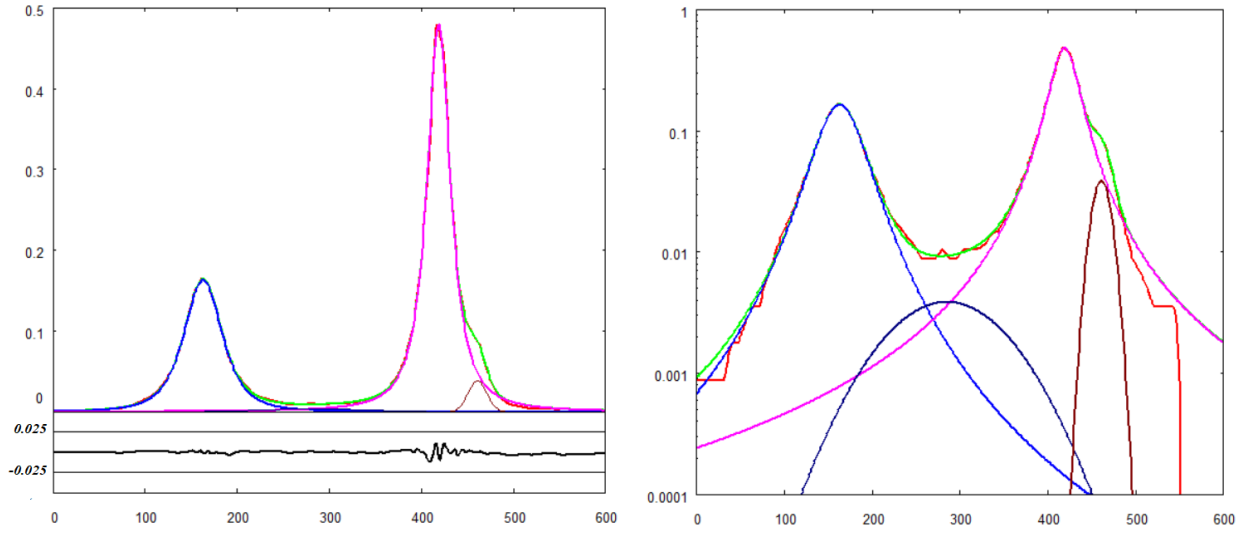

Fig. 11: The best fit (green) onto OSR2200 and q-Gaussian components, proposed also in the semi log scale (with increased n).

ResearchGate – At the following link, Interpretation of the 2D peak in a Raman spectra of graphite, 2015, Danny Ahumada, University of California, Santa Barbara, proposed two Raman spectra of graphite. One spectrum corresponds to a sample that he synthesized, the other is of commercial graphite. Here, let us consider the sample prepared by Ahumada: we can see a peak given at 1579 cm^{-1}, with a shoulder that we estimate at 1620 cm^{-1}. Then, we have the peak at 1350 cm^{-1}. Therefore, we consider just three bands.

Comparison - For comparison of the previously given data, let us assume the central positions of the peaks (in cm^{-1}), that we can observe in the spectra analyzed above, and given in the following table. For the spectrum provided by ROD, we propose the data as can be evaluated from the Fig.7, but also the positions of the center of the bands as obtained by the best fit (fit in the Fig.9, with four bands).

RRUFF-050503	-	1558	1584	-
RRUFF-090047	-	1556	1584	-
RRUFF-120025	1361	-	1581	1623
ROD-3500021 (Fig.7)	1350	-	1572	1606
ROD-3500021 (Fig.9)	1345	1550	1570	1604
OSR2200	1352	-	1583	1623
OSR1500	1346	1520	1578	1614
Ahumada's sample	1350	-	1579	1620

In the table given above we can see the presence of the D band at about 1350 cm^{-1} (this band is negligible in RRUFF 050503 and 090047), of the G band at about 1580 cm^{-1}, and of the shoulder of this band at about 1610-1620 cm^{-1} (note please the different behavior of RRUFF 050503 and 090047 and the different position of the G peak shoulder). We can see that the carbonization of biochar graphitized it (according to Tagliaferro et al., 2020). The presence of several elements, besides carbon, produces a band which appears between D and G bands (OSR1500); it seems something similar existing for OSR2200, but the component is so low and flat that we considered it negligible for comparison. In the case of ROD-3500021 we have this band, shifted towards the G band, so that we consider it as another shoulder of G peak (see Fig.9). As previously told, in the case of RRUFF 050503 and 090047 too, this band is a shoulder of the G band.

The G-band is the main Raman mode in graphite and graphene, linked to the planar configuration sp^2 bonded carbon, which is constituting the graphene layers (Application Note). "The band position is pretty much independent of excitation laser frequency" (Application Note). The D-band is the "disorder band" or the "defect band". "This band is linked to the ring breathing mode from sp^2 carbon rings … The band is typically very weak in graphite and is typically weak in graphene as well. If the D-band is significant, it indicates that there are a lot of defects in the material" (Application Note).

G' band

Here we continue the analysis by means of q-Gaussians of the G' band. Here in the following the results.

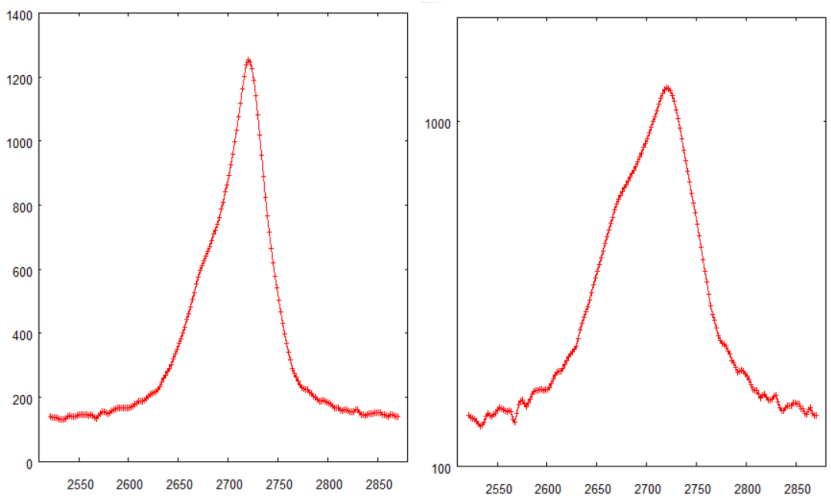

Fig. 12: Data of RRUFF 050503 of G' band. On the right, the data with log scale y-axis. On x-axis, we have Raman shift in cm^{-1}.

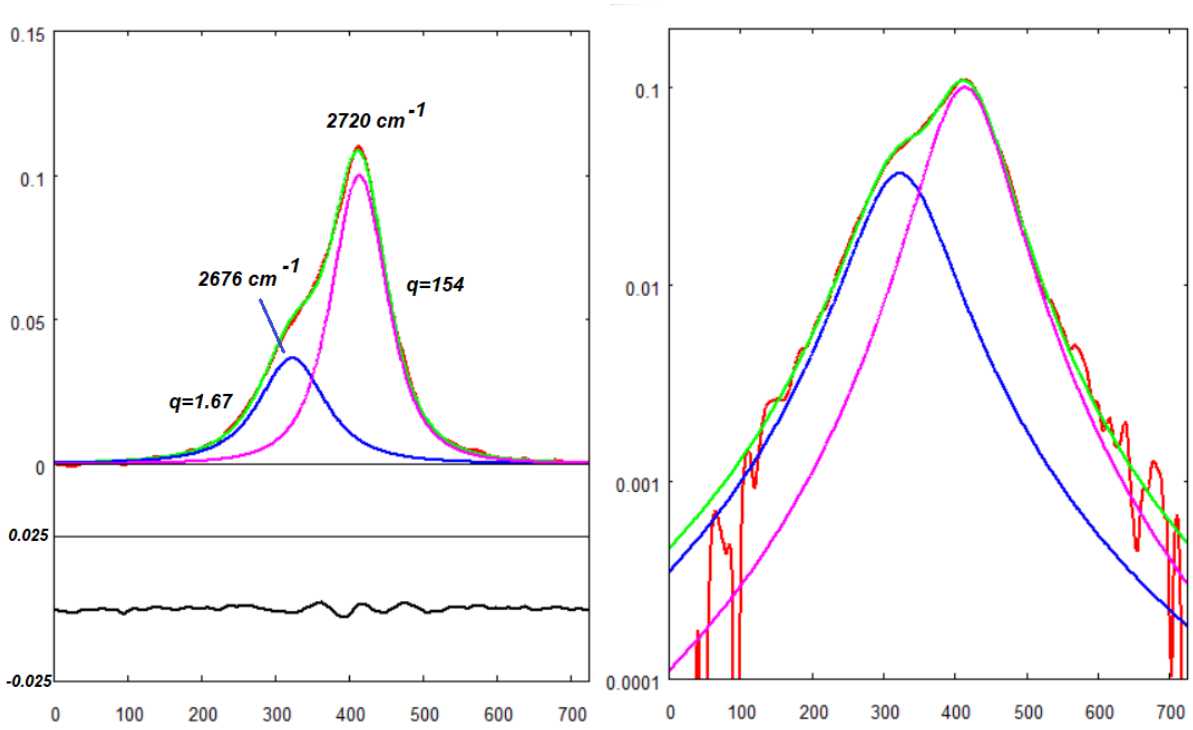

Fig. 13: The best fit (green) onto RRUFF 050503 and two q-Gaussian components.

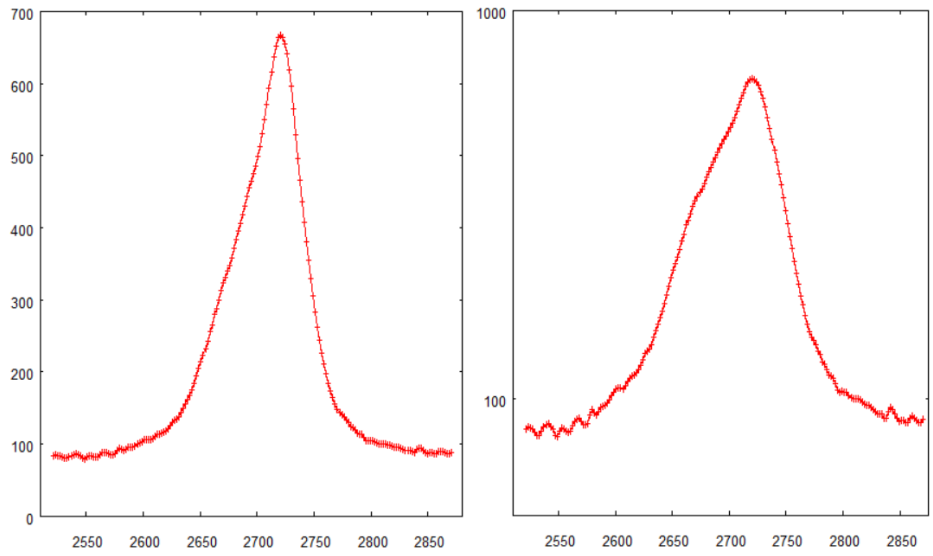

Fig. 14: Data of RRUFF 090047 of G' band. On the right, the data with log scale y-axis. On x-axis, we have Raman shift in cm^{-1}.

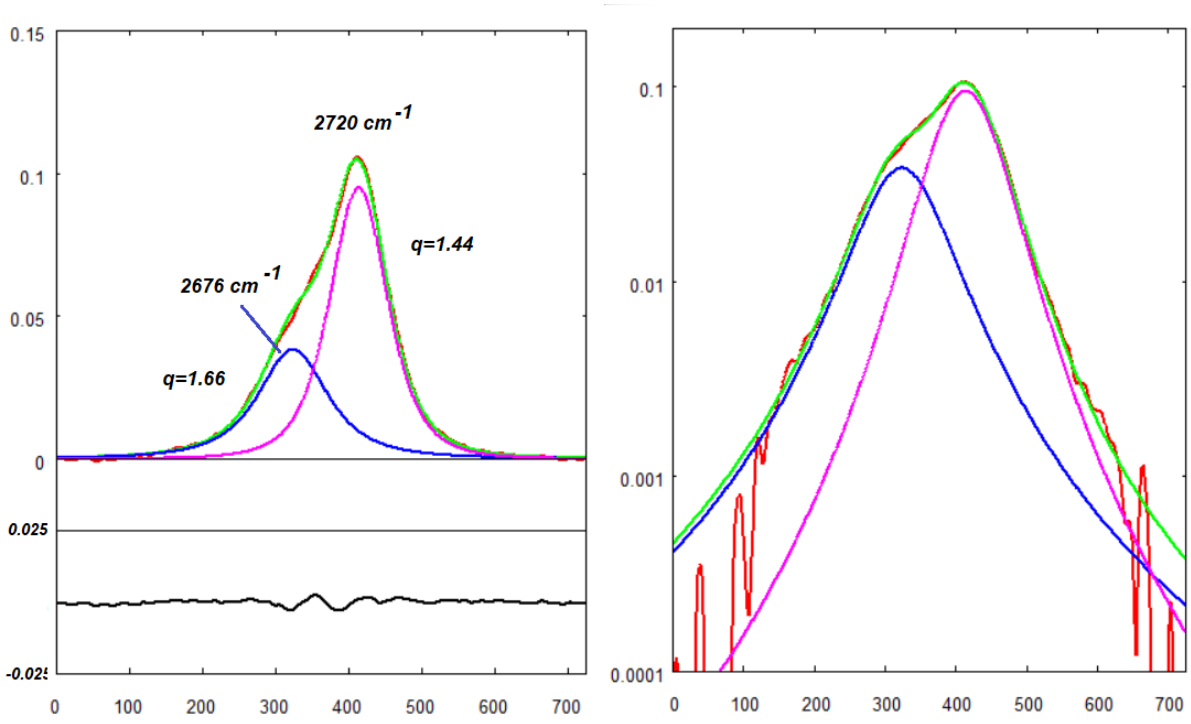

Fig. 15: The best fit (green) onto RRUFF 90047 and two q-Gaussian components.

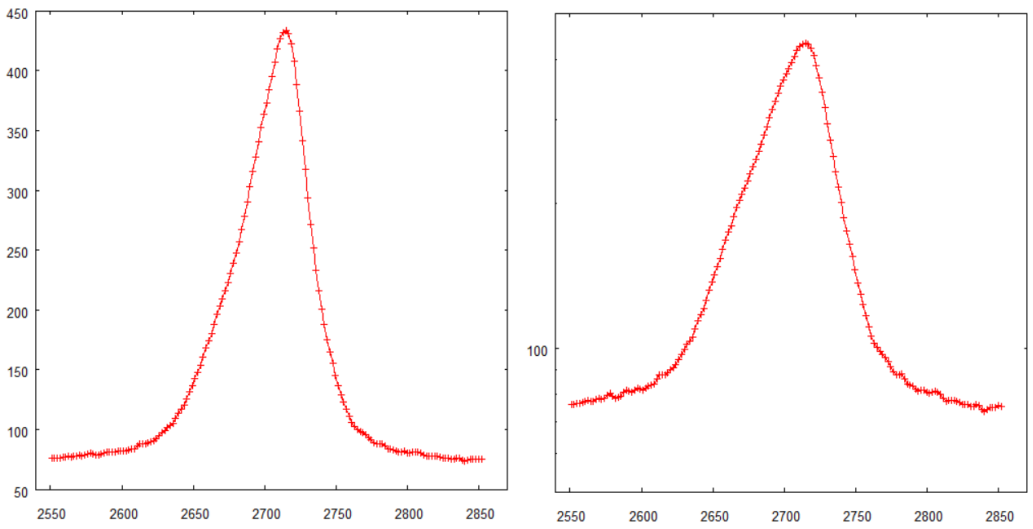

Fig. 16: Data of RRUFF 120025 of G' band. On the right, the data with log scale y-axis. On x-axis, we have Raman shift in cm^{-1}.

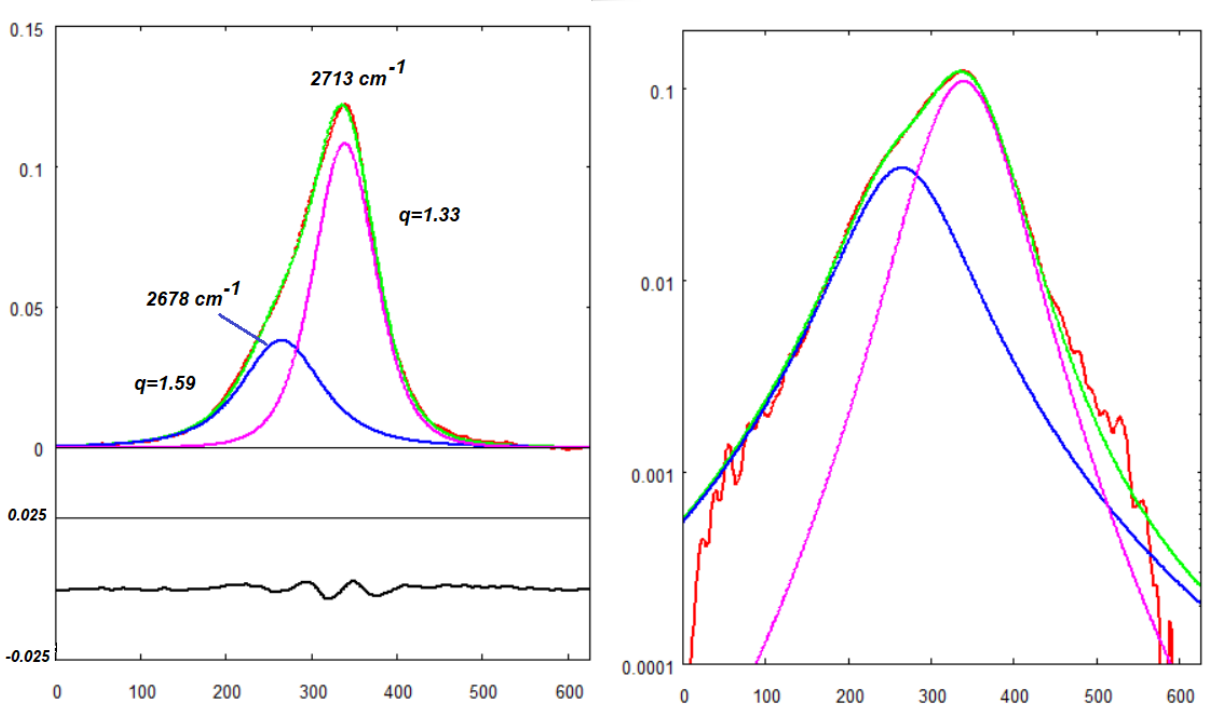

Fig. 17: The best fit (green) onto RRUFF 120025 and two q-Gaussian components.

About G' band, a fundamental reference is Malard et al., 2009. The main discussion is the Raman spectroscopy of graphene. "In the case of Bernal AB stacking of graphene …, Ferrari et al., 2006, showed that is possible to use the second order G' feature in the Raman spectra of graphene to learn about the number of layers in a graphene sample. As in other sp^2 carbons, the G' feature in the Raman spectrum originates from the double resonance (DR) Raman process", linking electrons and phonons in the graphene dispersion relations (Malard et al., 2009).

For the different stacking arrangements in graphite, see please the figure at the following ResearchGate link: https://www.researchgate.net/figure/Different-stacking-of-graphite-a-d-are-different-structures-of-graphite_fig6_261767193 , in an article by Liu et al., 2014.

Increasing the stacking of graphene layers, "the G' band continues to evolve with the number of layers until we reach the final material that we must consider which is bulk graphite. For highly oriented pyrolytic graphite (HOPG) … we can describe the G' band with two peaks" (see the Fig. 8(e) in Malard et al., 2009). In the Figure 8(e) by Malard et al., we can see the G' fitted with two profiles, which we can suppose being Lorentzian, because no different lineshapes are mentioned in the article. Caption of Fig.8 tells that plots are showing: "The measured G' Raman band with 2.41 eV laser energy for (a) 1-LG, (b) 2-LG, (c) 3-LG, (d) 4-LG, (e) HOPG and (f) turbostratic graphite. The splitting of the G' Raman band opens up in going from mono- to three-layer graphene and then closes up in going from 4-LG to HOPG". Unfortunately, panel 8(f), that related to turbostratic graphite, does not exist. Turbostratic graphite is also denoted as 2D graphite (Malard et al., 2009, page 52).

In Malard et al., we can find that it "is important to note that the identification of the number of layers by Raman spectroscopy is well established only for graphene samples that have AB Bernal stacking. Graphene samples made by the mechanical exfoliation of natural or HOPG graphite lead to graphene flakes that have predominantly AB stacking, but this is not necessarily the case for graphene samples made by other growth methods" (Malard et al., 2009). "For example, turbostratic graphite, in which the stacking of the graphene layers is rotationally random with respect to one another along the c axis …, shows a Raman G' band that

is a single Lorentzian (see Fig. 8(f) [actually, not given in the figure]), just as in monolayer graphene … but with a larger linewidth" (Malard et al., 2009). Moreover, "the absence of an interlayer interaction between the graphene planes makes the Raman spectra of turbostratic graphite look much like that for monolayer graphene. The reason for this is that the electronic structure for turbostratic graphite can be described in the same way as monolayer graphene, but now with a broadening of the G' feature …". (Malard et al., 2009. The broadening is associate with the random orientation of the layers with respect to each other, as told by Malard and coworkers.

Let us also add what is further told in the mentioned article by Malard et al., about G, D and G' bands. The most evident bands in the Raman spectra of graphene are the "so-called G band appearing at 1582 cm^{-1} (graphite) and the G' band at about 2700 cm^{-1} using laser excitation at 2.41 eV". If we have a "disordered sample or at the edge of a graphene sample, we can also see the so-called disorder-induced D-band, at about half of the frequency of the G' band (around 1350 cm^{-1} using laser excitation at 2.41 eV)" (Malard et al., 2009). "The G band is associated with the doubly degenerate (iTO [i for in-plane] and LO) phonon mode (E_{2g} symmetry) at the Brillouin zone center". Actually, as expressed by the authors, the G-band is "the only band coming from a normal first order Raman scattering process in graphene. On the other hand, the G' and D-bands originate from a second-order process, involving two iTO phonons near the K point for the G' band or one iTO phonon and *one defect* in the case of the D-band" (Malard et al., 2009).

About the G' band, since it is about twice the D band frequency, in literature we can find it also called as "2D" band. Again, let us stress that "this two-phonon band is allowed in the second order Raman spectra of graphenes without any kind of disorder or defects. In order to prevent any misleading connection of this feature with disorder or defects, and to avoid confusion between the designation of 2D to denote two dimensionality," the G' conventional notation is preferred by Malard and coworkers, 2009.

Remarks - In Sparavigna, 2023e, we considered the Tsallis q-Gaussian functions, compared to the Kaniadakis κ-Gaussian functions and applied to the analysis of diamond Raman spectrum. The Kaniadakis Gaussian is another generalization of the Gaussian function. We have shown that Tsallis Gaussians, Kaniadakis Gaussians and pseudo-Voigt functions are providing slightly different results. It is necessary to know the transfer function of the instrument to determine if it is possible to discriminate the results and decide the preferred function. It is also necessary to consider the manner the data have been processed and the role of the baseline. Without any information regarding processing, the Tsallis Gaussian fitting examples provided here and in Sparavigna, 2023c, show that we can use these functions to substitute pseudo-Voigt and Voigt functions. Let us stress that, in the frequency ranges here considered, processed and raw data of graphite RRUFF samples are the same.

Tsallis Gaussians can be easily compared with Gaussian and Lorentzian functions, and with pseudo-Voigtian functions too. In fact, for q-parameter equal to 2, the q-Gaussian is the Lorentzian function. In the case of the Kaniadakis Gaussians, the difference with Lorentzian function is appreciable in the far-wings, Therefore, being the q-Gaussians the natural generalization of Gaussians and Lorentzians, which are the functions more involved in the Raman spectral analysis, the use of Tsallis Gaussians must be preferred.
The semi log scale, that we have used for diamond and graphite Raman spectrum analyses is enhancing the far-wing behaviour, and this is relevant for distinguishing q-Gaussians from other functions. In the study of diamond Raman spectra, we noted that the far-wings of Kaniadakis Gaussians, pseudo-Voigt and Voigt functions seem being more "Lorentzian" that those of the Tsallis Gaussians. In the cases here proposed for graphite, we can see that the wings are properly described by q-Gaussians, and therefore no further functions have been considered for fitting.

References

1. Application Note. Characterizing graphene with Raman spectroscopy. Available https://web.archive.org/web/20220815105344/https://assets.thermofisher.com/TFSAssets/MSD/Application-Notes/AN53174-characterizing-graphene-raman-spectroscopy.pdf
2. Bartoli, M., & Giorcelli, M. (Eds.). (2022). Recent Perspectives in Pyrolysis Research. IntechOpen Editions.
3. Brassard, P., Godbout, S., Lévesque, V., Palacios, J. H., Raghavan, V., Ahmed, A., Hogue, R., Jeanne, T., & Verma, M. (2019). Biochar for soil amendment. In Char and carbon materials derived from biomass (pp. 109-146), Elsevier, 2019.
4. El Mendili, Y., Vaitkus, A., Merkys, A., Gražulis, S., Chateigner, D., Mathevet, F., Gascoin, S., Petit, S., Bardeau, J.-F., Zanatta, M., Secchi, M., Mariotto, G., Kumar, A., Cassetta, M., Lutterotti, L., Borovin, E., Orberger, B., Simon, P., Hehlen, B., & Le Guen, M. (2019). Raman Open Database: first interconnected Raman–X-ray diffraction open-access resource for material identification. Journal of Applied Crystallography, 52(3), 618-625. doi: 10.1107/s1600576719004229
5. Ferrari, A.C., Meyer, J.C., Scardaci, V., Casiraghi, C., Lazzeri, M., Mauri, F., Piscanec, S., Jiang, D., Novoselov, K.S., Roth, S., & Geim, A.K. (2006). Raman spectrum of graphene and graphene layers. Physical review letters, 97(18), p.187401.
6. Hanel, R., Thurner, S., & Tsallis, C. (2009). Limit distributions of scale-invariant probabilistic models of correlated random variables with the q-Gaussian as an explicit example. The European Physical Journal B, 72(2), 263.
7. Kaniadakis, G. (2013). Theoretical foundations and mathematical formalism of the power-law tailed statistical distributions. Entropy, 15(10), 3983-4010
8. Kirillov, S. A. (2004a). Novel approaches in spectroscopy of interparticle interactions. Raman line profiles and dynamics in liquids and glasses. Journal of molecular liquids, 110(1-3), 99-103.
9. Kirillov, S. (2004b). Novel approaches in spectroscopy of interparticle interactions. Vibrational line profiles and anomalous non-coincidence effects. In Novel Approaches to the Structure and Dynamics of Liquids: Experiments, Theories and Simulations; Springer: Berlin/Heidelberg, Germany, 2004; pp. 193–227
10. Lafuente, B., Downs, R. T., Yang, H., & Stone, N. (2015). 1. The power of databases: The RRUFF project. In Highlights in mineralogical crystallography (pp. 1-30). De Gruyter (O).
11. Liu, R., Chi, Y., Fang, L., Tang, Z., & Yi, X. (2014). Synthesis of carbon nanowall by plasma-enhanced chemical vapor deposition method. Journal of nanoscience and nanotechnology, 14(2), 1647-1657.
12. Malard, L. M., Pimenta, M. A., Dresselhaus, G., & Dresselhaus, M. S. (2009). Raman spectroscopy in graphene. Physics reports, 473(5-6), 51-87.
13. Meier, R. J. (2005). On art and science in curve-fitting vibrational spectra. Vibrational spectroscopy, 2(39), 266-269.
14. Merlen, A., Buijnsters, J. G., & Pardanaud, C. (2017). A guide to and review of the use of multiwavelength Raman spectroscopy for characterizing defective aromatic carbon solids: From graphene to amorphous carbons. Coatings, 7(10), 153.
15. Naudts, J. (2009). The q-exponential family in statistical physics. Central European Journal of Physics, 7, 405-413.
16. Rautian, S. G. (1958). Real spectral apparatus. Soviet Physics Uspekhi, 1(2), 245.
17. Seshadri, K., & Jones, R. N. (1963). The shapes and intensities of infrared absorption bands—A review. Spectrochimica Acta, 19(6), 1013-1085
18. Sparavigna, A. C. (2022). Entropies and Logarithms. Zenodo. DOI 10.5281/zenodo.7007520
19. Sparavigna, A. C. (2023a). q-Gaussian Tsallis Line Shapes and Raman Spectral Bands. International Journal of Sciences, 12(03), 27-40. http://dx.doi.org/10.18483/ijSci.2671

20. Sparavigna, A. C. (2023b). q-Gaussian Tsallis Functions and Egelstaff-Schofield Spectral Line Shapes. International Journal of Sciences, 12(03), 47-50. http://dx.doi.org/10.18483/ijSci.2673
21. Sparavigna, A. C. (2023c). q-Gaussian Tsallis Line Shapes for Raman Spectroscopy (June 7, 2023). SSRN Electronic Journal. http://dx.doi.org/10.2139/ssrn.4445044
22. Sparavigna, A. C. (2023d). Formamide Raman Spectrum and q-Gaussian Tsallis Lines (June 12, 2023). SSRN Electronic Journal. http://dx.doi.org/10.2139/ssrn.4451881
23. Sparavigna, A. C. (2023e). Tsallis and Kaniadakis Gaussian functions, applied to the analysis of Diamond Raman spectrum, and compared with Pseudo-Voigt functions. Zenodo. https://doi.org/10.5281/zenodo.8087464
24. Tagliaferro, A., Rovere, M., Padovano, E., Bartoli, M., & Giorcelli, M. (2020). Introducing the novel mixed gaussian-lorentzian lineshape in the analysis of the Raman signal of biochar. Nanomaterials, 10(9), 1748.
25. Tatum, J. (2022). Combination of Profiles. (2022, March 5). University of Victoria. https://phys.libretexts.org/@go/page/6710
26. Tsallis, C. (1988). Possible generalization of Boltzmann-Gibbs statistics. Journal of statistical physics, 52, 479-487.
27. Tsallis, C. (1995). Some comments on Boltzmann-Gibbs statistical mechanics. Chaos, Solitons & Fractals, 6, 539-559.
28. Umarov, S., Tsallis, C., Steinberg, S. (2008). On a q-Central Limit Theorem Consistent with Nonextensive Statistical Mechanics. Milan J. Math. Birkhauser Verlag. 76: 307–328. doi:10.1007/s00032-008-0087-y. S2CID 55967725.